An adaptive Strategy for the Multi-scale Analysis of Plate and Shell Structures with Elasto-plastic Material Behaviour

W. Wagner, F. Gruttmann

Modelling of structures on different scales has been a popular subject in the past. Within such a strategy the structural behaviour is modeled on a macro-level, describing the structure itself, whereas the material behaviour is modeled on a micro-level. Here typically RVEs are used. The proper choice of boundary conditions for the RVE is a difficult task in case of shell structures. It should be mentioned that the correct calculation of material parameters on the macro level is crucial for any associated nonlinear analysis. Here, results have been presented for homogeneous and layered structures for composite materials in Gruttmann and Wagner (2013). In the present paper we will discuss the influence of material nonlinear behaviour, here the elasto-plastic behaviour, within the above described setting. Typically these calculations are very time consuming, even if the FE-model is parallelized. Thus we will discuss possibilities to change material models on the structural model during the loading process, starting with elastic material models without a second scale and switching to a two-scale approach, where necessary.

1 Introduction

Finite shell elements which are based on the first–order shear deformation theory are in general able to describe the global deformation behaviour of thin plate and shell structures. However for some stress components only an average shape through the thickness can be obtained. Various methods have been developed to obtain the complicated local deformation behaviour in inhomogeneous thin structures. So–called multi–director shell formulations with an appropriate number of global degrees of freedom at the nodes yield approximate solutions of the three–dimensional boundary value problem, e.g. Reddy (2004). The application of brick elements or solid shell elements provides likewise a computationally expensive approach, e.g. Klinkel et al. (1999, 2006). For laminates each layer must be discretized with several elements in thickness direction to obtain satisfactory results. The numerical effort for such a full-scale solution leads for practical problems to an unreasonable number of unknowns. The enhancement of the displacement field by layer-wise linear (zig-zag) functions through the thickness, see e.g. Carrera (2003), could be another option. Applications for thin shell structures with a complicated 3D-stress state could be photovoltaic laminates, OLED, PLED devices, piecoeletric devices, thin CFRP-parts of lightweight structures in aerospace or automotive industry, among many others. In the present paper the shells are treated as a homogeneous continuum with effective properties obtained through a homogenization procedure to avoid large-scale computations. A large number of papers exists on computational homogenization methods for general heterogeneous materials, see e.g. Zohdi and Wriggers (2005); De Borst and Ramm (2011) for a survey and new developments. Computational homogenization procedures for thin structured sheets have been proposed in Geers et al. (2007); Coenen et al. (2010). The theory in Geers et al. (2007) is based on a Reissner–Mindlin kinematic, whereas in Coenen et al. (2010) a Kirchhoff-Love kinematic is adopted. Representative volume elements (RVE) extending through the full thickness of the structure are introduced. At the top and bottom surfaces of the RVE stress boundary conditions are applied, whereas periodicity constraints are applied at the lateral surfaces.

Based on these preliminaries the essential features and new aspects of the present formulation are summarized as follows:

(i) The underlying shell formulation based on the Reissner–Mindlin theory with inextensible director field is summarized. A two-scale model is introduced and a variational formulation and associated linearization for the coupled global–local boundary value problem is presented.

(ii) For the solution of the two-scale problem a FE^2 method for small strains is described. Quadrilateral elements are used for the discretization of the shell structure, whereas solid shell elements are applied on the RVE, which extends through the total thickness of the shell. A relation between in–plane displacements and shell strains is developed on the lateral surfaces.

(iii) The nonlinear coupled local and global boundary value problems are simultaneously solved in a Newton iteration scheme.

(iv) An indicator, based on ideas in Zienkiewicz and Zhu (1987), is developed which allows the switch between different material models. Thus the FE^2 method is only used, where it should be necessary. The approach of changing material models is fully reversible. Thus, unloading is possible.
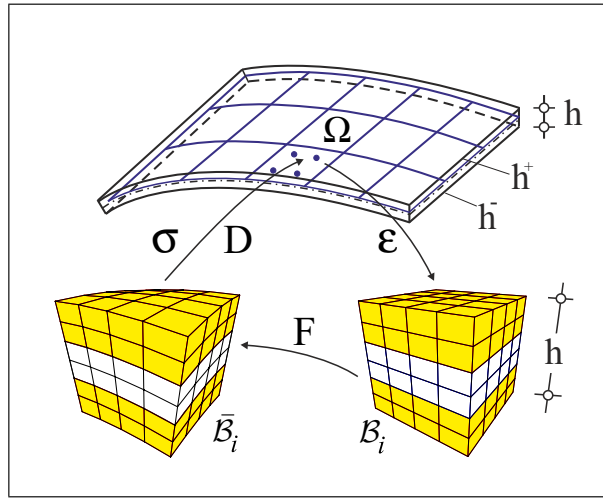
2 Two-scale Shell Model – Theory

Figure 1. Computational homogenization of a layered shell

Let $\mathcal{B}$ be the three–dimensional Euclidean space occupied by a shell with thickness h in the reference configuration. With ξ^i we denote a convected coordinate system of the body. The thickness coordinate $\xi^3 = z$ is defined in the range $h^- \leq z \leq h^+$, where h^- and h^+ are the z–coordinates of the outer surfaces. Thus, an arbitrary reference surface Ω with boundary Γ is introduced. The shell is loaded statically by loads $\bar{\mathbf{p}}$ in Ω and by boundary forces $\bar{\mathbf{t}}$ on Γ_σ. In the following Greek indices range from 1 to 2 and commas denote partial differentiation with respect to ξ^α.

Position vectors of the initial reference surface and current surface are denoted by $\mathbf{X}(\xi^\alpha)$ and $\mathbf{x}(\xi^\alpha)$, respectively. Furthermore, a director $\bar{\mathbf{D}}(\xi^\alpha)$ with $|\bar{\mathbf{D}}(\xi^\alpha)| = 1$ is introduced as a vector field perpendicular to Ω. The unit director field $\bar{\mathbf{d}}(\xi^\alpha)$ of the current configuration is obtained by orthogonal transformations and is a function of the rotational parameters $\bar{\boldsymbol{\omega}}$. Within the Reissner–Mindlin theory transverse shear strains are accounted for, thus $\bar{\mathbf{d}} \cdot \mathbf{x},_\alpha \neq 0$.

Hence, the displacement field follows from the difference of the position vectors in shell space

$$\bar{\mathbf{u}} = \bar{\mathbf{u}}_0 + z\,(\bar{\mathbf{d}} - \bar{\mathbf{D}}) \qquad\qquad \bar{\mathbf{u}}_0 = \mathbf{x} - \mathbf{X}\,. \tag{1}$$

The shell strains are derived from the Green–Lagrangian strain tensor using kinematic assumption (1) and are arranged in a vector as

$$\boldsymbol{\varepsilon}(\bar{\mathbf{u}}_0, \bar{\boldsymbol{\omega}}) = [\varepsilon_{11}, \varepsilon_{22}, 2\,\varepsilon_{12}, \kappa_{11}, \kappa_{22}, 2\,\kappa_{12}, \gamma_1, \gamma_2]^T\,, \tag{2}$$

with the membrane strains $\varepsilon_{\alpha\beta}$, curvatures $\kappa_{\alpha\beta}$ and transverse shear strains γ_α, respectively.

According to Fig. 1 a representative volume element (RVE) at an integration point i of a typical finite shell element is introduced. The domain $\mathcal{B}_i$ extends through the total thickness h of the shell and has the size $l_x \times l_y \times h$.

The displacement field is split in an averaged part $\bar{\mathbf{u}}$ and a fluctuation part $\tilde{\mathbf{u}}$.

$$\mathbf{u} = \bar{\mathbf{u}} + \tilde{\mathbf{u}} \tag{3}$$

The averaged displacements $\bar{\mathbf{u}}$ according to (1) are a linear function of the thickness coordinate, whereas $\tilde{\mathbf{u}}$ describes warping and thickness change. Hence, the deformation gradient $\mathbf{F} = \mathbf{1} + \mathrm{Grad}\,\mathbf{u}$ is defined in a standard way and the Green–Lagrangian strain tensor follows from $\mathbf{E} = \frac{1}{2}(\mathbf{F}^T \mathbf{F} - \mathbf{1})$.

The weak form of equilibrium can now be written with $\mathbf{v} = [\bar{\mathbf{u}}_0, \bar{\boldsymbol{\omega}}, \mathbf{u}]^T$ and admissible variations $\delta\mathbf{v} = [\delta\bar{\mathbf{u}}_0, \delta\bar{\boldsymbol{\omega}}, \delta\mathbf{u}]^T$

$$g(\mathbf{v}, \delta\mathbf{v}) = \int_{\Omega} (\boldsymbol{\sigma} \cdot \delta\boldsymbol{\varepsilon} - \bar{\mathbf{p}} \cdot \delta\bar{\mathbf{u}}_0)\, dA - \int_{\Gamma_\sigma} \bar{\mathbf{t}} \cdot \delta\bar{\mathbf{u}}_0\, ds + \sum_{e=1}^{ne2} \sum_{i=1}^{NGP} \frac{1}{A_i} \int_{\Omega_i} \int_{h^-}^{h^+} \mathbf{S} : \delta\mathbf{E}\, \bar{\mu}\, dz\, dA = 0. \tag{4}$$

Here, $\boldsymbol{\sigma}$ denotes the vector of stress resultants

$$\boldsymbol{\sigma} = [n^{11}, n^{22}, n^{12}, m^{11}, m^{22}, m^{12}, q^1, q^2]^T \tag{5}$$

with membrane forces $n^{\alpha\beta} = n^{\beta\alpha}$, bending moments $m^{\alpha\beta} = m^{\beta\alpha}$ and shear forces q^α. On the RVE's $\mathbf{S}$ denotes the Second Piola-Kirchhoff stress tensor with $\mathbf{P} = \mathbf{F}\,\mathbf{S}$ and the virtual Green-Lagrangian strain tensor is introduced via $\delta\mathbf{E} = \frac{1}{2}(\delta\mathbf{F}^T \mathbf{F} + \mathbf{F}^T \delta\mathbf{F})$. Furthermore $ne1$ and $ne2$ denote the number of shell elements without or with a two-scale model introduced. NGP is the number of Gauss points for each element and $A_i = l_x\, l_y$ is the reference area of the RVE. It holds for the total number of shell elements: $ne = ne1 + ne2$.

For the finite element formulation of the next section we need to derive the linearization of eq. (4). With conservative loads $\bar{\mathbf{p}}$ and $\bar{\mathbf{t}}$ one obtains

$$L\left[g(\mathbf{v}, \delta\mathbf{v}), \Delta\mathbf{v}\right] := g(\mathbf{v}, \delta\mathbf{v}) + Dg \cdot \Delta\mathbf{v} \tag{6}$$

where $g(\mathbf{v}, \delta\mathbf{v})$ is given in (4) and

$$Dg \cdot \Delta\mathbf{v} = \int_{\Omega} (\Delta\boldsymbol{\sigma} \cdot \delta\boldsymbol{\varepsilon} + \boldsymbol{\sigma} \cdot \Delta\delta\boldsymbol{\varepsilon})\, dA + \sum_{e=1}^{ne2} \sum_{i=1}^{NGP} \frac{1}{A_i} \int_{\Omega_i} \int_{h^-}^{h^+} (\Delta\mathbf{S} : \delta\mathbf{E} + \mathbf{S} : \Delta\delta\mathbf{E})\, \bar{\mu}\, dz\, dA \tag{7}$$

with $\Delta\boldsymbol{\sigma} = \mathbf{D}\,\Delta\boldsymbol{\varepsilon}$, $\Delta\mathbf{S} = \mathbf{C}\,\Delta\mathbf{E}$ and $\Delta\delta\mathbf{E} = \frac{1}{2}(\delta\mathbf{F}^T \Delta\mathbf{F} + \Delta\mathbf{F}^T \delta\mathbf{F})$. The material matrix $\mathbf{C}$ is a standard output of a library of constitutive laws in a material description. The linearized virtual shell strains $\Delta\delta\boldsymbol{\varepsilon}$ are derived for finite rotations in Wagner and Gruttmann (2005). The stress resultant vector $\boldsymbol{\sigma}$ and the matrix of linearized stress resultants $\mathbf{D}$ are specified in the next section.

3 Two-scale Shell Model – Finite Element Formulation

We describe a finite element formulation based on a standard displacement method applying the isoparametric concept. The reference surface of the shell is discretized with ne quadrilateral isoparametric shell elements

$$\Omega^h = \sum_{e=1}^{ne1} \Omega_e + \sum_{e=1}^{ne2} \Omega_e\,, \tag{8}$$

where the subscript h refers to the finite element approximation. Initial geometry, displacements and rotations are interpolated with bilinear functions $N_I(\xi, \eta)$ which are arranged in the matrix $\mathbf{N}$. The nodal degrees of freedom are three displacements and two or three rotations.

Inserting the interpolation functions for the displacements and virtual displacements into the linearized weak form (6) considering (4) and (7) yields

$$
L\left[g(\mathbf{v}^h, \delta\mathbf{v}^h), \Delta\mathbf{v}^h\right] = \sum_{e=1}^{ne1} \delta\mathbf{v}_e^G \mathbf{k}_e^G \Delta\mathbf{v}_e^G + \mathbf{f}_e^G
$$

$$
+ \sum_{e=1}^{ne2}
\begin{bmatrix}
\delta\mathbf{v}^G \\
\delta\mathbf{V}_1 \\
\vdots \\
\delta\mathbf{V}_i \\
\vdots \\
\delta\mathbf{V}_{NGP}
\end{bmatrix}_e^T
\left\{
\begin{bmatrix}
\mathbf{k}^G & \mathbf{0} & \vdots & \mathbf{0} & \vdots & \mathbf{0} \\
\mathbf{0} & \mathbf{K}_1^L & \vdots & \mathbf{0} & \vdots & \mathbf{0} \\
\cdots & \cdots & \ddots & \mathbf{0} & \cdots & \cdots \\
\mathbf{0} & \mathbf{0} & \mathbf{0} & \mathbf{K}_i^L & \mathbf{0} & \mathbf{0} \\
\cdots & \cdots & \cdots & \mathbf{0} & \ddots & \cdots \\
\mathbf{0} & \mathbf{0} & \cdots & \mathbf{0} & \cdots & \mathbf{K}_{NGP}^L
\end{bmatrix}_e
\begin{bmatrix}
\Delta\mathbf{v}^G \\
\Delta\mathbf{V}_1 \\
\vdots \\
\Delta\mathbf{V}_i \\
\vdots \\
\Delta\mathbf{V}_{NGP}
\end{bmatrix}_e
+
\begin{bmatrix}
\mathbf{f}^G(\boldsymbol{\sigma}_i) \\
\mathbf{F}_1^L \\
\vdots \\
\mathbf{F}_i^L \\
\vdots \\
\mathbf{F}_{NGP}^L
\end{bmatrix}
\right\}_e
\qquad (9)
$$

The indices G and L refer to the global and local boundary value problems, respectively. The matrices of the first row in (9) follow from the global part of the linearized weak form. The element residual vector and the tangential element stiffness matrix read

$$
\mathbf{f}^G(\boldsymbol{\sigma}_i) = \int_{(\Omega_e)} (\mathbf{B}^T\boldsymbol{\sigma} - \mathbf{N}^T\bar{\mathbf{p}})\, dA - \int_{(\Gamma_{\sigma e})} \mathbf{N}^T\bar{\mathbf{t}}\, ds
\qquad\qquad
\mathbf{k}^G(\mathbf{D}_i) = \int_{(\Omega_e)} (\mathbf{B}^T\mathbf{D}\,\mathbf{B} + \mathbf{G})\, dA \quad (10)
$$

where the matrices $\mathbf{B}$ and $\mathbf{G}$ are derived in Wagner and Gruttmann (2005). The vector of stress resultants $\boldsymbol{\sigma}_i$ and linearized stress resultants $\mathbf{D}_i$ are specified below.

The matrices of the second to the last row in (9) are associated with the local boundary value problems at Gauss points $1 \le i \le NGP$ of shell element e and occur only, if a two-scale model is used.

A local boundary value problem can be defined at Gauss point i

$$
\delta\mathbf{V}_i^T \left(\mathbf{K}_i^L \Delta\mathbf{V}_i + \mathbf{F}_i^L\right) = \frac{1}{A_i} \sum_{e=1}^{Ne} \delta\mathbf{v}_e^T (\mathbf{k}_e^L \Delta\mathbf{v}_e + \mathbf{f}_e^L)\,.
\qquad (11)
$$

Here, the total number of elements used for the discretization of the RVE is denoted by Ne. The element residual vector $\mathbf{f}_e^L$ and the tangential element stiffness matrix $\mathbf{k}_e^L$ read

$$
\mathbf{f}_e^L = \int_{(V_e)} \tilde{\mathbf{B}}^T\mathbf{S}\, dV
\qquad\qquad
\mathbf{k}_e^L = \int_{(V_e)} (\tilde{\mathbf{B}}^T\mathbf{C}\,\tilde{\mathbf{B}} + \tilde{\mathbf{G}})\, dV\,.
\qquad (12)
$$

where $\tilde{\mathbf{B}}$ and $\tilde{\mathbf{G}}$ are the virtual strain displacement matrix and the geometrical matrix of 8–noded solid shell elements, respectively.

The element displacement vector $\mathbf{v}_e$ is now split in a part $\mathbf{v}_\Omega$ which contains the internal displacements and a part $\mathbf{v}_\Gamma$ which contains the boundary displacements of the RVE.

$$
\mathbf{v}_e =
\begin{bmatrix}
\mathbf{v}_\Omega \\
\mathbf{v}_\Gamma
\end{bmatrix}
=
\begin{bmatrix}
\mathbf{v}_a \\
\mathbf{v}_b
\end{bmatrix}
=
\begin{bmatrix}
\mathbf{a}_e\,\mathbf{V}_i \\
\mathbf{A}_e\,\boldsymbol{\varepsilon}_i
\end{bmatrix}
\qquad (13)
$$

In Eq. (13) $\mathbf{a}_e$ is the standard assembly matrix and $\mathbf{A}_e(x, y, z)$ will be specified in the following.

Assuming small strains the relation of the boundary displacements to the averaged strains $\bar{\mathbf{E}}$ is written as

$$
\begin{bmatrix}
\bar{u}_x \\
\bar{u}_y \\
\bar{u}_z
\end{bmatrix}
=
\begin{bmatrix}
\bar{E}_{11} & \bar{E}_{12} & \bar{E}_{13} \\
\bar{E}_{21} & \bar{E}_{22} & \bar{E}_{23} \\
\bar{E}_{31} & \bar{E}_{32} & \bar{E}_{33}
\end{bmatrix}
\begin{bmatrix}
x \\
y \\
z
\end{bmatrix}.
\qquad (14)
$$

Inserting the relation of the averaged strains to the shell strains

$$
\begin{array}{rcl}
\bar{E}_{11} & = & \varepsilon_{11} + z\,\kappa_{11} \\
\bar{E}_{22} & = & \varepsilon_{22} + z\,\kappa_{22} \\
\bar{E}_{33} & = & 0 \\
\bar{E}_{12} & = & \bar{E}_{21} = \varepsilon_{12} + z\,\kappa_{12} \\
2\,\bar{E}_{13} & = & 2\,\bar{E}_{31} = 2\,\varepsilon_{13} = \gamma_1 \\
2\,\bar{E}_{23} & = & 2\,\bar{E}_{32} = 2\,\varepsilon_{23} = \gamma_2
\end{array}
\tag{15}
$$

into (14) yields with further considerations, see Gruttmann and Wagner (2013),

$$
\left[\begin{array}{c} \bar{u}_x \\ \bar{u}_y \end{array} \right] = \left[\begin{array}{ccc} \varepsilon_{11} + z\kappa_{11} & \varepsilon_{12} + z\kappa_{12} & 2\,\varepsilon_{13} \\ \varepsilon_{12} + z\kappa_{12} & \varepsilon_{22} + z\kappa_{22} & 2\,\varepsilon_{23} \end{array} \right] \left[\begin{array}{c} x \\ y \\ z \end{array} \right]
\tag{16}
$$

Eq. (16) is now rewritten with the vector of shell strains (2) as

$$
\left[\begin{array}{c} \bar{u}_x \\ \bar{u}_y \end{array} \right] = \left[\begin{array}{cccccccc} x & 0 & \frac{1}{2}y & xz & 0 & \frac{1}{2}yz & z & 0 \\ 0 & y & \frac{1}{2}x & 0 & yz & \frac{1}{2}xz & 0 & z \end{array} \right] \left[\begin{array}{c} \varepsilon_{11} \\ \varepsilon_{22} \\ 2\varepsilon_{12} \\ \kappa_{11} \\ \kappa_{22} \\ 2\kappa_{12} \\ \gamma_1 \\ \gamma_2 \end{array} \right]
\tag{17}
$$

$$
\bar{\mathbf{u}}_I = \mathbf{A}_I(x,y,z)\,\boldsymbol{\varepsilon}\,,
$$

where the index refers to node I of the considered element e. The matrices $\mathbf{A}_I$ are submatrices of $\mathbf{A}_e$ introduced in (13)

$$
\mathbf{A}_e = \left[\begin{array}{c} \delta_1\,\mathbf{A}_1 \\ \vdots \\ \delta_I\,\mathbf{A}_I \\ \vdots \\ \delta_{nel}\,\mathbf{A}_{nel} \end{array} \right]_{(2\,nel \times 8)} \qquad \delta_I = \left\{ \begin{array}{ll} 1 & \text{if node } I \text{ has fixed dofs} \\ 0 & \text{else} \end{array} \right.
\tag{18}
$$

with $nel = 8$ for 8–noded solid shell elements.

Introducing $\mathbf{k}_{\alpha\beta}$ and $\mathbf{f}_\alpha$ with $\alpha, \beta = a, b$ as submatrices of $\mathbf{k}_e^L$ and $\mathbf{f}_e^L$ in (11) leads to

$$
\delta\mathbf{V}_i^T\,(\mathbf{K}_i^L\,\Delta\mathbf{V}_i + \mathbf{F}_i^L)
$$

$$
= \frac{1}{A_i} \sum_{e=1}^{Ne} \left[\begin{array}{c} \delta\mathbf{V}_i \\ \delta\boldsymbol{\varepsilon}_i \end{array} \right]^T \left\{ \left[\begin{array}{cc} \mathbf{a}_e^T\,\mathbf{k}_{aa}\,\mathbf{a}_e & \mathbf{a}_e^T\,\mathbf{k}_{ab}\,\mathbf{A}_e \\ \mathbf{A}_e^T\,\mathbf{k}_{ba}\,\mathbf{a}_e & \mathbf{A}_e^T\,\mathbf{k}_{bb}\,\mathbf{A}_e \end{array} \right]_e \left[\begin{array}{c} \Delta\mathbf{V}_i \\ \Delta\boldsymbol{\varepsilon}_i \end{array} \right] + \left[\begin{array}{c} \mathbf{a}_e^T\,\mathbf{f}_a \\ \mathbf{A}_e^T\,\mathbf{f}_b \end{array} \right]_e \right\}
\tag{19}
$$

$$
= \frac{1}{A_i} \left[\begin{array}{c} \delta\mathbf{V}_i \\ \delta\boldsymbol{\varepsilon}_i \end{array} \right]^T \left\{ \left[\begin{array}{cc} \mathbf{K} & \mathbf{L} \\ \mathbf{L}^T & \mathbf{M} \end{array} \right] \left[\begin{array}{c} \Delta\mathbf{V}_i \\ \Delta\boldsymbol{\varepsilon}_i \end{array} \right] + \left[\begin{array}{c} \mathbf{F}_a \\ \mathbf{F}_b \end{array} \right] \right\}\,.
$$

With $\delta\mathbf{V}_i \neq \mathbf{0}$ the internal degrees of freedom $\Delta\mathbf{V}_i$ can be eliminated from the set of equations using

$$
\mathbf{K}\,\Delta\mathbf{V}_i + \mathbf{L}\,\Delta\boldsymbol{\varepsilon}_i + \mathbf{F}_a = \mathbf{0}
\tag{20}
$$

which yields

$$
\Delta\mathbf{V}_i = -\mathbf{K}^{-1}\,(\mathbf{F}_a + \mathbf{L}\,\Delta\boldsymbol{\varepsilon}_i)\,.
\tag{21}
$$

With (20) and (21) eq. (19) reduces to

$$\delta \mathbf{V}_i^T \left(\mathbf{K}_i^L \, \Delta \mathbf{V}_i + \mathbf{F}_i^L \right) \quad = \quad \delta \boldsymbol{\varepsilon}_i^T \left(\mathbf{D}_i \, \Delta \boldsymbol{\varepsilon}_i + \boldsymbol{\sigma}_i \right) \tag{22}$$

where

$$\boldsymbol{\sigma}_i = \frac{1}{A_i} (\mathbf{F}_b - \mathbf{L}^T \, \mathbf{K}^{-1} \, \mathbf{F}_a) \qquad\qquad \mathbf{D}_i = \frac{1}{A_i} (\mathbf{M} - \mathbf{L}^T \, \mathbf{K}^{-1} \, \mathbf{L}) \tag{23}$$

are the stress resultants and linearized stress resultants of Gauss point i. Finally (22) is inserted into the linearized coupled global-local boundary value problem (9)

$$
L\left[g(\mathbf{v}^h, \delta\mathbf{v}^h), \Delta\mathbf{v}^h\right] = \sum_{e=1}^{ne1} \delta\mathbf{v}_e^G \mathbf{k}_e^G \Delta\mathbf{v}_e^G + \mathbf{f}_e^G
$$

$$
+ \sum_{e=1}^{ne2}
\begin{bmatrix}
\delta\mathbf{v}^G \\
\delta\boldsymbol{\varepsilon}_1 \\
\vdots \\
\delta\boldsymbol{\varepsilon}_i \\
\vdots \\
\delta\boldsymbol{\varepsilon}_{NGP}
\end{bmatrix}_e^T
\left\{
\begin{bmatrix}
\mathbf{k}^G(\mathbf{D}_i) & \mathbf{0} & \vdots & \mathbf{0} & \vdots & \mathbf{0} \\
\mathbf{0} & \mathbf{D}_1 & \vdots & \mathbf{0} & \vdots & \mathbf{0} \\
\dots & \dots & \ddots & \mathbf{0} & \dots & \dots \\
\mathbf{0} & \mathbf{0} & \mathbf{0} & \mathbf{D}_i & \mathbf{0} & \mathbf{0} \\
\dots & \dots & \dots & \mathbf{0} & \ddots & \dots \\
\mathbf{0} & \mathbf{0} & \dots & \mathbf{0} & \dots & \mathbf{D}_{NGP}
\end{bmatrix}_e
\begin{bmatrix}
\Delta\mathbf{v}^G \\
\Delta\boldsymbol{\varepsilon}_1 \\
\vdots \\
\Delta\boldsymbol{\varepsilon}_i \\
\vdots \\
\Delta\boldsymbol{\varepsilon}_{NGP}
\end{bmatrix}_e
+
\begin{bmatrix}
\mathbf{f}^G(\boldsymbol{\sigma}_i) \\
\boldsymbol{\sigma}_1 \\
\vdots \\
\boldsymbol{\sigma}_i \\
\vdots \\
\boldsymbol{\sigma}_{NGP}
\end{bmatrix}_e
\right\}_e
\tag{24}
$$

The coupled nonlinear system of equations is simultaneously solved within a Newton iteration scheme. The iteration is terminated for the actual load step when local equilibrium in all Gauss points is attained along with the global equilibrium of the shell which is formulated through the first row of (9) or (24). For further details, see Gruttmann and Wagner (2013).

4 Adaptive Strategy for the use of different material models

As already said the calculation of structures with a two-scale model is very time consuming. Thus an interesting strategy could be to use the same 2D nonlinear shell element together with different material laws at different load levels. Within this paper we have in mind

- Non layered shell structure with linear elastic material law-MAT1 (EL)

- Layered shell structure with elasto-plastic material law-MAT4 (ELPL) (only for test reasons)

- Non layered shell structure with a two-scale FE^2-model on elements $0 \leq e \leq ne2$ with RVE on each Gauss point-MAT8 (RVE + ELPL)

Thus a calculation starts fully elastic with MAT1 (EL) on a non layered structure. During the loading process a switch to a layered structure with an elasto-plastic material-MAT4 (ELPL) or to a RVE with elasto-plastic material-MAT8 (RVE + ELPL) is introduced. This switching procedure requires an indicator to decide if a material change is necessary. In earlier times the indicator of Zienkiewicz and Zhu (1987) has been successfully used in different applications for an adaptive mesh refinement. A typical formulation is

$$\int \Delta\mathbf{S}^T \Delta\mathbf{S} \, dA \geq \alpha \|E_\sigma\| \,, \tag{25}$$

where $\|E_\sigma\|$ is an averaged system energy based on FE-stresses $\mathbf{S}_{GP}$ calculated at Gauss points

$$\|E_\sigma\| = \frac{1}{ne} \sum_{e=1}^{ne} \int \mathbf{S}_{GP}^T \mathbf{S}_{GP} \, dA \,. \tag{26}$$

Based on a standard FE-smoothing procedure nodal stresses $\mathbf{S}_N$ could be provided, which can be used to calculate stress differences $\Delta\mathbf{S} = \mathbf{S}_N - \mathbf{S}_{GP}$ on each element e. If the first term in Eq. (25) is larger then the second one a

mesh refinement will be necessary. Typical $\alpha = 0.05$ can be used, which means that an error of 5% is admissible in one element.

In the same sense one could introduce similar expressions within a nonlinear elasto-plastic model. A first attempt is the simple model

$$\int S_V^2 \, dA \geq \alpha \|E_\sigma\| \quad \text{and} \quad \|E_\sigma\| = \frac{1}{ne} \sum_{e=1}^{ne} \int Y_0^2 \, dA \tag{27}$$

with a yield stress Y_0 and the equivalent stress $S_V = \sqrt{S_{11}^2 - S_{11} S_{22} + S_{22}^2 + 3 S_{12}^2}$. Now, if the first term exceeds the second one a change of the material model will be necessary. Typical $\alpha = 0.9$ is a possible choice, which means the elastic domain is admissible in one element up to 90% of the yield stress. The material model is changed for the whole element, if the above described condition is violated once during the loops on layers and Gauss points. In case of the elasto-plastic material, stresses are calculated naturally at each layer. Using the two-scale model the output of the RVE are stress resultants, see Eqs. (5, 23). Thus the stress values at top and bottom of the shell have to be calculated in a standard way via

$$S_{ii+} = \frac{n_{ii}}{h} + \frac{m_{ii}}{I_i} z_+ \,, \quad S_{ii-} = \frac{n_{ii}}{h} + \frac{m_{ii}}{I_i} z_- \,. \tag{28}$$

Using the above strategy in a parallelized FE-code needs a dynamic parallelization of the element loop. Thus a balancing of the workload of each processor is necessary due to the fact that elements with elastic material behaviour as well as elements with another elasto-plastic FE-model on each Gauss-point occur.

LOOP, Load

LOOP, Iteration(Newton)

LOOP, Element (Stiffness matrix and residual)
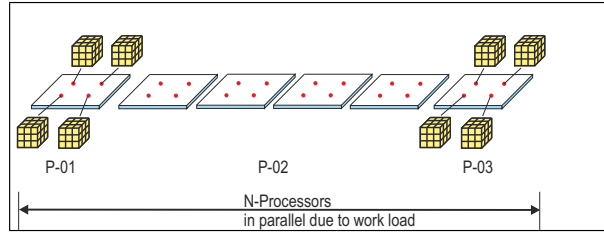
NEXT, Element
SOLVE $\mathbf{K}_T \Delta \mathbf{V} = -\mathbf{R}$ with Parallel-Solver

NEXT, Iteration

NEXT, Load

Further informations on the parallelization of an element loop in a FE-code may be found e.g. in Jarzebski et al. (2015).

5 Unloading

Special attention has to be set on possible unloading behaviour. Typically the process of changing the material model should be reversible. Thus a switch back to a fully elastic material model must be possible. Having in mind that elasto-plastic strains have been reached earlier a general material model $\boldsymbol{\sigma}_{ep} = \mathbf{D}(\boldsymbol{\varepsilon} - \boldsymbol{\varepsilon}_p)$ for the stress resultants is necessary. Hence the question is how to calculate elasto-plastic shell strains $\boldsymbol{\varepsilon}_p$ and elasto-plastic stress resultants $\boldsymbol{\sigma}_{ep}$.

For the elasto-plastic material- MAT4 (ELPL) one can calculate the stress resultants $\boldsymbol{\sigma}_{ep}$ in a loop over all layers

at each Gauss point from the 3D-stresses $\mathbf{S}_{ep}$.

$$
\begin{aligned}
&\boldsymbol{\sigma}_{ep} = 0\,, \mathbf{D}_{ep} = 0 \\
&i = 1, nlay \\
&\quad \rightarrow \mathbf{E}_i = \boldsymbol{\varepsilon}_m + z_i \boldsymbol{\kappa} \\
&\quad \leftarrow \mathbf{S}_{i\,ep} = \mathbf{C}_{i\,ep}\mathbf{E}_i \qquad \text{store for } i\ :\ \mathbf{E}_{i\,p}, E_{i\,v} \\
&\boldsymbol{\sigma}_{ep} = \boldsymbol{\sigma}_{ep} + \int\limits_z \mathbf{S}_{i\,ep}\,dz_i \\
&\mathbf{D}_{ep} = \mathbf{D}_{ep} + \int\limits_z \mathbf{C}_{i\,ep}\,dz_i \\
&\text{end } i
\end{aligned}
\tag{29}
$$

In case of the two-scale model-MAT8 all shell values are calculated directly on the RVE at each Gauss point.

$$
\begin{aligned}
&\rightarrow \quad \boldsymbol{\varepsilon} \quad\ = [\boldsymbol{\varepsilon}_m, \boldsymbol{\kappa}, \boldsymbol{\gamma}] \\
&\leftarrow \quad \boldsymbol{\sigma}_{ep} \ = [\mathbf{N}_{ep}, \mathbf{M}_{ep}, \mathbf{Q}_{ep}] \qquad \text{store on RVE: } \mathbf{E}_p, E_v \\
&\leftarrow \quad \mathbf{D}_{ep}
\end{aligned}
\tag{30}
$$

Thus, in case of unloading, the elasto-plastic strains

$$
\boldsymbol{\varepsilon}_p = \boldsymbol{\varepsilon} - \mathbf{D}_{ep}^{-1}\boldsymbol{\sigma}_{ep}
\tag{31}
$$

are stored in a history array and the switch to the fully elastic material-MAT1 can be done via

$$
\boldsymbol{\sigma} = \mathbf{D}(\boldsymbol{\varepsilon} - \boldsymbol{\varepsilon}_p)
\tag{32}
$$

6 Examples

The developed algorithms are implemented in an extended version of the general finite element program FEAP Taylor (2011). With the first example we compare the finite element solutions for a Two-span girder subjected to concentrated loads with analytical expressions. The same is done within the second example for a square plate.

6.1 Two-span girder with single loads

For the first example we choose a simple Two-span girder with single loads. The length is given with $L = 100$ cm and the cross section data are $B = 10$ cm, $H = 2$ cm. The external loading is given by two 2 single loads $F = f \cdot B = 1$ kN. For the material law we introduce a classical elasto-plastic material behaviour including linear hardening. We choose the elasticity modulus $E = 21000$ kN/cm^2, Poisson's ratio $\nu = 0.3$, initial yield strength $Y_0 = 30$ kN/cm^2 and the hardening modulus $C_p = E/10000$ kN/cm^2. An analytical solution (without hardening) including unloading is available on the basis of a plastic hinge theory. The distribution of the bending moments in the ultimate load case is presented in Figure 2 with 3 plastic hinges.
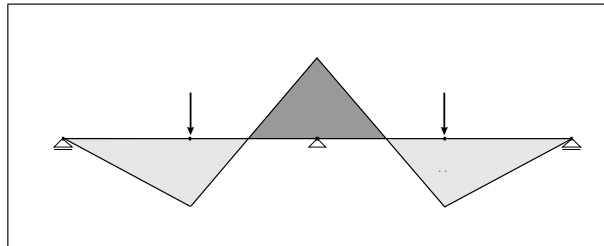

Figure 2. Bending moments of 2-span girder with single loads

The associated finite element discretization is presented in Figure 3, taking into account that symmetry conditions could be used. The mesh is chosen with 40 4-node shell elements in length direction and 4 elements in transverse direction, respectively. The element formulation is based on a finite rotation theory including an interface to different 2D- and 3D-material formulations, for details see Wagner and Gruttmann (2005).
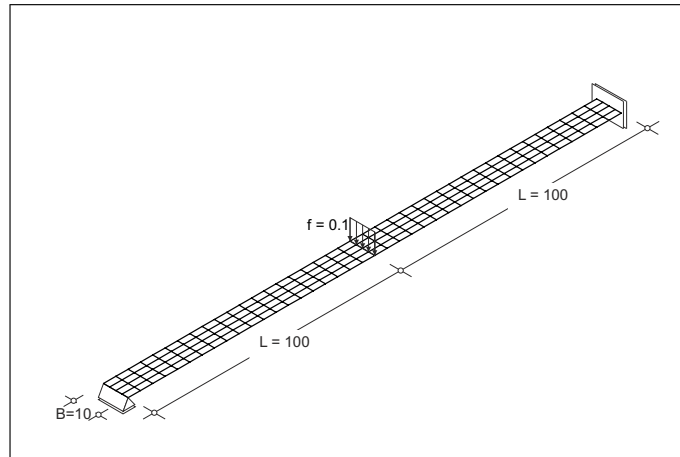
Figure 3. FE-discretization of the symmetric part 2-span girder with single loads

In Figure 4 load deflection curves are presented. These are depicted for the single load versus the vertical displacement under the single load. Curves are shown based on an analytical solution from the plastic hinge beam theory with $F_{pht} = Y_0(BH^2/6L)(4+1) = 9$ kN. First results are from a FE-model shell with elasto-plastic material behaviour (MAT4) and 11 layers in thickness direction. Second results are from a shell formulation with a multiscale FE^2 approach (MAT8), see Gruttmann and Wagner (2013), describing the macroscopic behaviour on the shell model and the elasto-plastic material behaviour (MAT4) on a representative volume model (RVE), introduced at each Gauss point on the shell level. The RVE has a size of $l_x = l_y = h$ and a discretization of $4 \times 4 \times 11$ solid shell elements, see Klinkel et al. (2006). Finally, for comparison, we present results introducing a 3D FE-model, again with the solid shell element mentioned before. Here, we choose for the 3D-mesh 11 elements in thickness direction. All results are very close together in the elastic range. Due to different geometrical discretization models slightly different results occur, especially in the plastic range, which leads to the same unloading behaviour starting from different points.
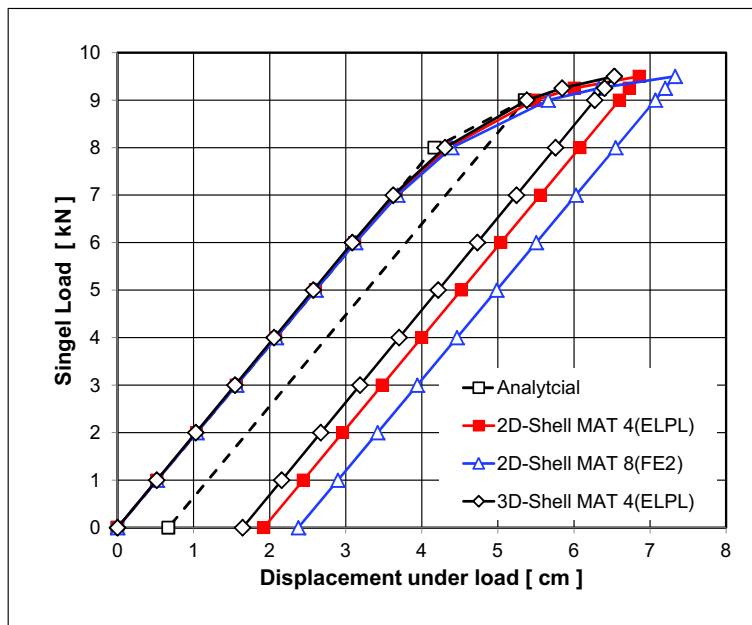

Figure 4. Load deflection curves for different models without changing the material model

Figure 5 depicts two load deflection curves when using the change of material models based on the above introduced error indicator. These curves are on one hand for the switch between elastic(MAT1) and elasto-plastic material behaviour (MAT4) and on the other hand for the switch between elastic (MAT1) and elasto-plastic material behaviour (MAT4) on a representative volume model (RVE). Both curves are in perfect agreement with load deflection curves without changing the material models. Presenting the unloading behaviour demonstrates, that the material switching procedure holds in both directions. The distribution of material models on the FE-mesh is visualized in Figure 6. Here, we can see finite elements with elastic(red) and elasto-plastic material(blue) on the

RVE at load levels for F=6/7/8/9/9.25/9.5/9.25/9.0 kN.
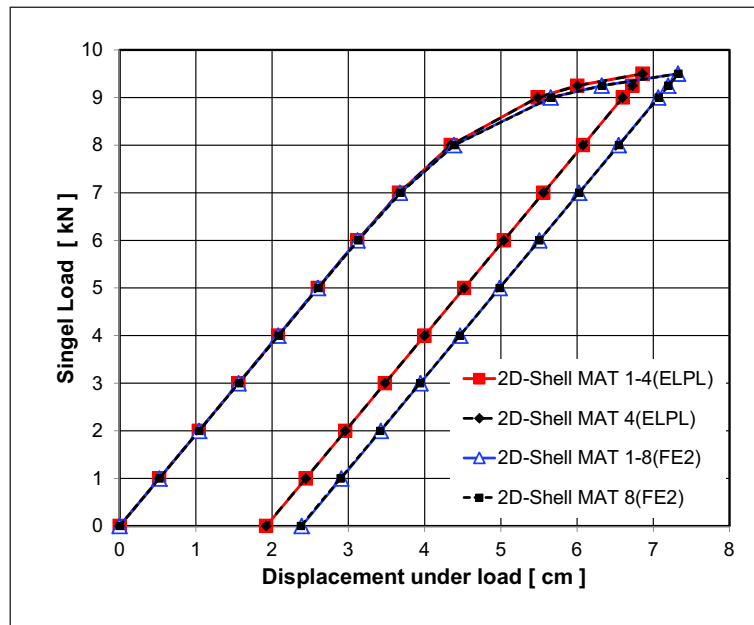

Figure 5. Load deflection curves for different models with change of the material model

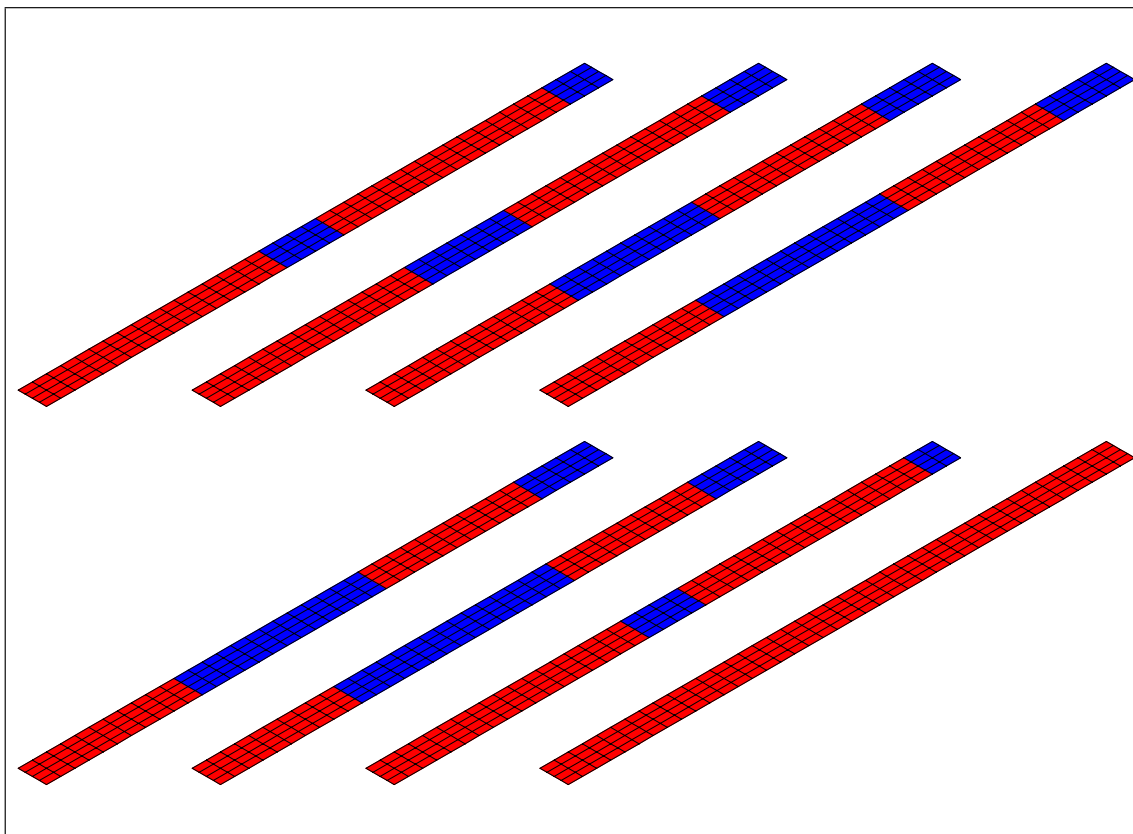Figure 6. Elements with elastic (red) and elasto-plastic material (blue) at different load levels for F=6/7/8/9/9.25/9.5/9.25/9.0 kN (top to bottom, left to right)

6.2 Square plate with uniform load

With the second example we discuss the elasto-plastic behaviour of a simply supported square plate with uniform load, see Figure 7. The length is given with $L_x = L_y = 200$ cm and the thickness is $h = 4$ cm. The external uniform load is given by $q = 1$ N/cm^2. For the material law we introduce again a classical elasto-plastic material

behaviour including linear hardening with material parameters of the last example, but with an initial yield strength of $Y_0 = 36$ kN/cm^2.
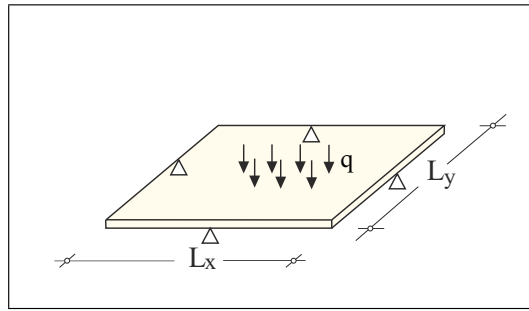

Figure 7. Simply supported square plate with uniform load

For the associated finite element discretization a mesh with 40 4-node shell elements, is chosen in both directions. Possible symmetry conditions are not taken into account. In Figure 8 load deflection curves for the value of the uniform load versus the vertical center displacement are presented. An analytical solution (without hardening) is available on the basis of a yield line theory with $q_{ylt} = 6Y_0 \cdot (h/L_x)^2 = 86.4$ N/cm^2. First results are from a FE-model shell with elasto-plastic material behaviour (MAT4) and 11 layers in thickness direction. Second results are from a FE-model shell with a multi-scale FE^2 approach (MAT8) describing the macroscopic behaviour on the shell model and the elasto-plastic material behaviour (MAT4) on a representative volume model (RVE), introduced at each Gauss point on the shell level. The RVE has a size of $l_x = l_y = h$ and a discretization of $4 \times 4 \times 5$ solid shell elements. Finally, for comparison, we present 3D-results using the solid shell element. Here, we choose for the 3D-mesh 5 elements in thickness direction. Associated element types have been described in the example before. All results are very close together in the elastic range. Due to different geometrical discretization models slightly different results occur, especially in the plastic range, which leads to the same unloading behaviour starting from different points. The different use of material models on the FE-mesh is visualized in Figure 9. The distribution of finite elements with elastic (red) and elasto-plastic material (blue) on the RVE is presented at load levels q=40/50/60/80/82.5/87.5/82.5/80/77.5 N/cm^2 (top to bottom, left to right). The typical behaviour with plastic effects along the diagonals ('yield lines') can be seen clearly.
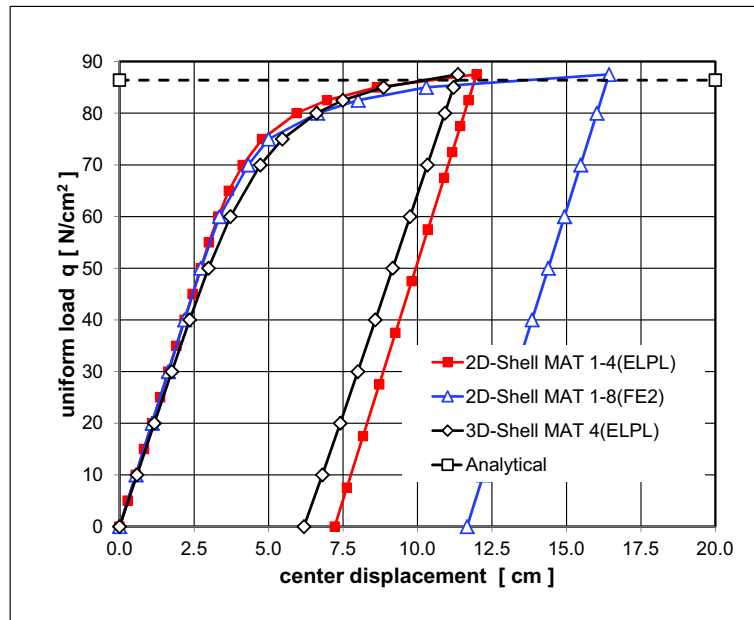

Figure 8. Load deflection curves for different discretizations and material models.

7 Conclusions

In this paper a multi-scale approach for shell structures is presented. With respect to shells the introduced RVE on the element Gauss point has a natural thickness h. This requires the formulation of special boundary conditions. The total set of equations contain equilibrium formulations on the structural level as well as on the level of Gauss points. It is possible to solve the whole set of equations simultaneously. Basically the formulation allows the mixture of element concepts. We have shown that it is possible to mix elements with conventional material description with elements, where RVE's are introduced to describe the material behaviour. Calculations based on a multi-scale approach are very time consuming. Thus an adaptive strategy has been introduced to switch automatically between different discretization and material models. For this an indicator in dependence on the indicator of Zienkiewicz and Zhu (1987) has been proposed. The examples show the efficient practical applicability of the proposed method, also in the unloading regime. Further research may be focused on the formulation of indicators to switch between different material models.
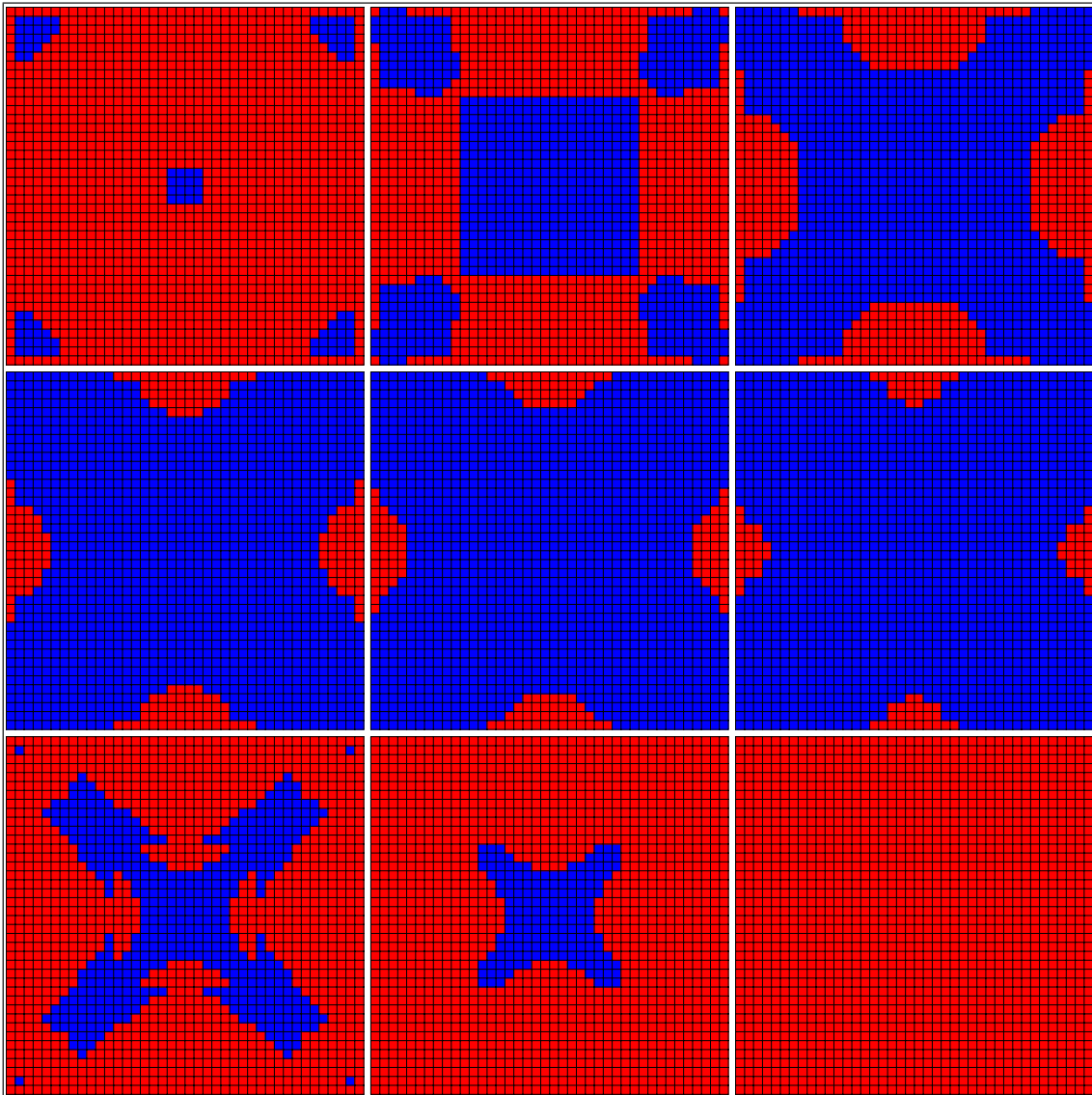

Figure 9. Elements with elastic (red) and elasto-plastic material (blue) at different load levels for q=40/50/60/80/82.5/87.5/82.5/80/77.5 N/cm^2 (top to bottom, left to right)

References

Carrera, E.: Historical review of zig-zag theories for multilayered plates and shells. *Appl. Mech. Reviews*, 56, (2003), 237 – 308.

Coenen, E.; Kouznetsova, V.; Geers, M.: Computational homogenization for heterogeneous thin sheets. *Int. J. Num. Meth. Engng.*, 83, (2010), 1180 – 1205.

De Borst, R.; Ramm, E.: *Multiscale methods in computational mechanics: progress and accomplishments, Springer Series: Lecture Notes in Applied and Computational Mechanics 55*. Springer, Berlin Heidelberg (2011).

Geers, M.; Coenen, E.; Kouznetsova, V.: Multi–scale computational homogenization of structured thin sheets. *Modelling Simul. Mater. Sci. Eng.*, 15, (2007), S393 – S404.

Gruttmann, F.; Wagner, W.: A coupled two-scale shell model with applications to layered structures. *Int. J. Num. Meth. Engng.*, 94, (2013), 1233 – 1254.

Jarzebski, P.; Wisniewski, K.; Taylor, R. L.: On parallelization of the loop over elements in FEAP. *Comput. Mech.*, 56, (2015), 77 – 86.

Klinkel, S.; Gruttmann, F.; Wagner, W.: A continuum based 3d–shell element for laminated structures. *Comp. & Struct.*, 71, (1999), 43–62.

Klinkel, S.; Gruttmann, F.; Wagner, W.: A robust non–linear solid shell element based on a mixed variational formulation. *Comp. Meth. Appl. Mech. Engrg.*, 195, (2006), 179 – 201.

Reddy, J. N.: *Mechanics of Laminated Composite Plates and Shells: Theory and Analysis*. CRC Press, London (2004).

Taylor, R.: Feap user manual, http://www.ce.berkeley.edu/projects/feap/manual.pdf.

Wagner, W.; Gruttmann, F.: A robust nonlinear mixed hybrid quadrilateral shell element. *Int. J. Num. Meth. Engng.*, 64, (2005), 635 – 666.

Zienkiewicz, O.; Zhu, J.: A simple error estimator and adaptive procedure for practical engineering analysis. *Int. J. Num. Meth. Engng.*, 24, (1987), 337 – 357.

Zohdi, T.; Wriggers, P.: *Introduction to Computational Micromechanics, Springer Series: Lecture Notes in Applied and Computational Mechanics 20*. Springer, Berlin Heidelberg (2005).

Address: Institut für Baustatik, Karlsruhe Institute of Technology, Kaiserstr. 12, D-76131 Karlsruhe
email: `w.wagner@kit.edu`